

## Mesoscale modeling of microgel mechanics and kinetics through the swelling transition\*

S. NIKOLOV<sup>1</sup>, A. FERNANDEZ-NIEVES<sup>2</sup>, A. ALEXEEV<sup>1,†</sup>

1. Woodruff School of Mechanical Engineering, Georgia Institute of Technology, Atlanta, GA 30332, U. S. A.;
  2. School of Physics, Georgia Institute of Technology, Atlanta, GA 30332, U. S. A.
- (Received Sept. 24, 2017 / Revised Nov. 10, 2017)

**Abstract** The mechanics and swelling kinetics of polymeric microgels are simulated using a mesoscale computational model based on dissipative particle dynamics. Microgels are represented by a random elastic network submerged in an explicit viscous solvent. The model is used to probe the effect of different solvent conditions on the bulk modulus of the microgels. Comparison of the simulation results through the volume phase transition reveals favorable agreement with Flory-Rehner's theory for polymeric gels. The model is also used to examine the microgel swelling kinetics, and is found to be in good agreement with Tanaka's theory for spherical gels. The simulations show that, during the swelling process, the microgel maintains a nearly homogeneous structure, whereas deswelling is characterized by the formation of chain bundles and network coarsening.

**Key words** soft matter, dissipative particle dynamics, micromechanics, hydrogels

**Chinese Library Classification** O631

**2010 Mathematics Subject Classification** 65C35, 82C80, 82B26

### 1 Introduction

Hydrogels have become a highly promising platform for developing novel microscale and nanoscale technologies, especially in biomedical engineering, where they are used as advanced drug delivery vehicles, microscopic manipulators/sensors, and scaffolds to regrow bones, muscles, and organs<sup>[1]</sup>. Recent experiments show that by varying the relaxation rates of the underlying hydrogel matrix, mesenchymal stem cells can be predisposed towards osteogenic differentiation (vs. adipogenic differentiation), which is important for bone tissue formation<sup>[2]</sup>. Methacrylated gelatin (MG) scaffolds have been used to regrow cardiac muscle cells<sup>[3]</sup>. It has been shown that by enriching the MG network with carbon nanotubes, the beating frequency of the cells could be varied. Hydrogels have also been used extensively to create novel drug

\* Citation: Nikolov, S., Fernandez-Nieves, A., and Alexeev, A. Mesoscale modeling of microgel mechanics and kinetics through the swelling transition. *Applied Mathematics and Mechanics (English Edition)*, 39(1), 47–62 (2018) <https://doi.org/10.1007/s10483-018-2259-6>

† Corresponding author, E-mail: [alexander.alexeev@me.gatech.edu](mailto:alexander.alexeev@me.gatech.edu)

Project supported by the National Science Foundation of U. S. A. (Nos. DMR-1255288, DMR-1609841, and DGE-1650044)

delivery devices. A new hydrogel-based micro-device capable of aiding diabetics by delivering a sustained release of insulin in response to enzymatic oxidation of glucose has been recently demonstrated<sup>[4]</sup>. Microscopic hydrogel particles have been used to encapsulate living cells to create three-dimensional (3D) micro-environments for cell culturing<sup>[5]</sup> and for controlled release of DNA targets<sup>[6]</sup>. Ultrasoft microgels have been shown to act as artificial platelets facilitating blood clotting<sup>[7]</sup>, whereas dense colloidal suspensions of such microgels enable assays to evaluate cell invasiveness<sup>[8]</sup>. In addition, stimuli-responsive multi-layered gel structures are promising for microactuator applications<sup>[9–11]</sup> and for designing self-propelling robots<sup>[12–14]</sup>.

Given the overwhelming potential of hydrogels, our aim is to develop a mesoscopic computational model, which can accurately capture the mechanical properties and swelling kinetics of microgel particles through the volume-phase transition, thereby facilitating the use of hydrogels in practical applications. The development of mesoscale models has attracted significant attention thanks to their ability to consider intermediate spatial and time scales that pose difficulties for more conventional atomistic and macroscopic (continuous) descriptions. Atomistic models provide a great wealth of detailed information regarding gel hydration and swelling<sup>[15]</sup>. However, the applications in the relevant nm- $\mu$ m length scales are typically not computationally accessible with atomistic simulations, hindering the potential utility in solving engineering problems. Continuous approaches enable access to much larger length and time scales compared with atomistic models. In this case, however, connecting individual chain parameters to bulk material properties is not an easy task for hydrogel materials<sup>[16]</sup> due to the complex interplay among elastic, hydrodynamic, and chemical interactions. As a result, mesoscale models of polymeric materials are gaining popularity due to their ability to tackle problems inaccessible by other methods<sup>[17–19]</sup>.

In this work, we examine a mesoscale hydrogel model based on dissipative particle dynamics (DPD). We focus on neutral hydrogel networks, and probe how individual chain parameters affect bulk gel properties in solvents of different quality. In particular, we examine how the bulk modulus changes through the volume-phase transition of microgel particles, and compare the simulation results with predictions from Flory-Rehner’s theory. Finally, we employ our mesoscale model to simulate the kinetics of spherical microgel particles during swelling and deswelling transitions and pinpoint important differences in microgel microstructure along these processes.

## 2 Methodology

We use DPD, a particle-based method where beads represent mesoscale molecular clusters and fluid volumes<sup>[20–22]</sup>, to model a mesoscale polymeric network immersed in a viscous solvent. The beads follow Newtonian dynamics and interact via soft potentials allowing a larger time step for the integration of the equation of motion. This in turn enables modeling systems over extended time scales, which are unachievable with atomistic methods. Furthermore, DPD uses pairwise interactions that preserve local hydrodynamics critical for modeling systems involving fluid flows. DPD has long been successfully tested against scaling theories for modeling simple systems<sup>[23–30]</sup> and experimental data<sup>[31–39]</sup>, showing that it can capture relevant physical effects.

The governing dynamics between beads in DPD is set by three main forces

$$\mathbf{F} = \sum_{j \neq i} (\mathbf{F}_{ij}^{\text{C}} + \mathbf{F}_{ij}^{\text{D}} + \mathbf{F}_{ij}^{\text{R}}),$$

acting between a given bead  $i$  and its neighboring bead  $j$  located within a cutoff radius  $r_c$ . There is a conservative repulsive force

$$\mathbf{F}_{ij}^{\text{C}} = a_{ij} w(r_{ij}) \hat{\mathbf{r}}_{ij},$$

which leads to the bead excluded volume, a dissipative force

$$\mathbf{F}_{ij}^D = -\gamma w(r_{ij})^2 (r_{ij} \cdot v_{ij}) \hat{\mathbf{r}}_{ij}$$

representing the effects of viscosity, and a random force

$$\mathbf{F}_{ij}^R = \sigma w(r_{ij}) \xi_{ij} (\Delta t)^{-1/2} \hat{\mathbf{r}}_{ij}$$

associated with thermal fluctuations. The latter two forces are related by

$$\sigma^2 = 2\gamma k_B T$$

due to the fluctuation-dissipation theorem. In all forces,  $w(r_{ij}) = 1 - \hat{r}_{ij}$  is a weighing function with

$$\hat{r}_{ij} = r_{ij}/r_c, \quad r_{ij} = |\mathbf{r}_i - \mathbf{r}_j|.$$

Additionally,  $\hat{\mathbf{r}}_{ij} = (\mathbf{r}_i - \mathbf{r}_j)/r_{ij}$ ,  $\xi_{ij}$  is a standard normal variable with zero mean,  $k_B$  is the Boltzmann constant, and  $T$  is the temperature.

To model the polymeric chains in the microgels, we use a bead-spring model (see Fig. 1(a)), where DPD beads are connected using a harmonic bond potential, a bending angle potential, and a segmented-repulsive potential (SRP). The energy for the bond potential is given by

$$U_{\text{bond}} = k_{\text{bond}}(r - r_{\text{eq}})^2,$$

where  $k_{\text{bond}}$  is the bond stiffness, and  $r_{\text{eq}}$  is the equilibrium separation length between beads. The energy for the angle potential is given by

$$U_{\text{bend}} = k_{\text{bend}}(1 + \cos \theta),$$

where  $k_{\text{bend}}$  is the bending stiffness, and  $\theta$  is the angle between two polymer bonds sharing a common bead. The segmented repulsive potential prevents polymer chains from crossing each other. It is implemented by imposing a soft repulsive force between chain bonds. The associated force is given by

$$\mathbf{F}_{ij}^{\text{SRP}} = C(1 - r_{\text{min}}/r_{\text{CSR P}}) \hat{\mathbf{r}}_{ij},$$

where  $r_{\text{CSR P}}$  is the cutoff distance for the SRP potential,  $r_{\text{min}}$  is the minimum distance between two bonds, and  $C$  is the strength of the potential<sup>[40]</sup>.

In our simulations, we set

$$\begin{cases} r_c = 1, & \gamma = 4.5, & k_B T = 1, & \rho = 3, \\ r_{\text{CSR P}} = 0.5, & C = 100, & \Delta t = 0.01. \end{cases}$$

Here,  $\rho$  is the number density of DPD beads in the system, and  $\Delta t$  is the simulation time step. The repulsions between solvent beads and between beads within polymer chains is

$$a_{\text{s-s}} = 25, \quad a_{\text{p-p}} = 25.$$

To model swelling and deswelling of the polymer gel, we alter the polymer-solvent repulsion  $a_{\text{p-s}}$  in the range between 20 and 35. For the sake of simplicity in what follows, we use  $a$  without a subscript to indicate the polymer-solvent repulsion, i.e.,  $a \equiv a_{\text{p-s}}$ . The bond stiffness for the polymer chains is set to  $k_{\text{bond}} = 35$  with  $r_{\text{eq}} = 0.6$ . The bending stiffness is set to  $k_{\text{bend}} = 10$ , except for the single chain simulations where  $k_{\text{bend}}$  varies in the range between 0 and 10. Note that all dimensional parameters are expressed in DPD units, unless indicated otherwise.

To create the gel network, we randomly distribute 3 600 crosslink points in a cubic box<sup>[38]</sup>. We then find all crosslink points separated by a distance in the range between  $0.8r_{\text{eq}}N$  and  $1.1r_{\text{eq}}N$ , and randomly connect them with connectivity up to 4 with straight polymer chains. Here,  $N$  is the average number of monomers per chain. The number of monomers in each chain is set such that the distance between beads is close to  $r_{\text{eq}}$ . A microgel with spherical shape is formed from the initial cubic gel by cutting out the chains outside the gel radius, with disconnected chain segments removed via a depth-first search algorithm<sup>[41]</sup> (see Fig. 1(b)). The final average connectivity is found to be about 3.4, mainly due to free chains at the outer gel surface.

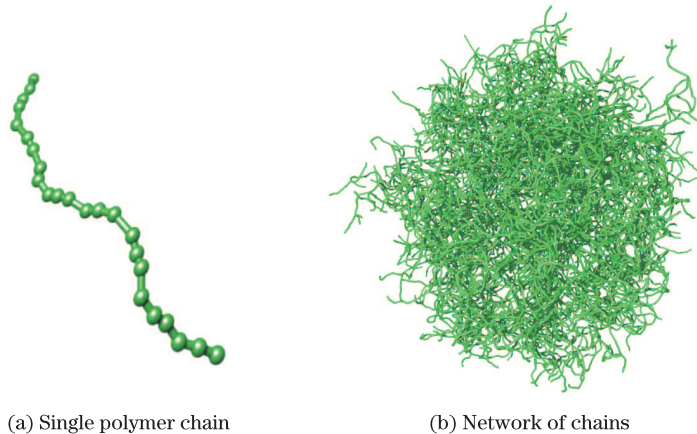


**Fig. 1** (a) Single polymer chain comprised of polymer beads connected with harmonic bonds. (b) Model of microgel network composed of individual chains interconnected at crosslinking sites (color online)

For all the microgel networks in our simulations, we use an identical initial crosslinking configuration. We investigate the effect of the number of beads per chain by setting  $N = 6, 9, 12,$  and  $24$ . To create networks with different  $N$ , we rescale the relative positions of crosslink points such that the average number of the monomers in the chains connecting them is close to the desired value. Thus, all networks share the same characteristics including the number of crosslinks, connectivity, and entanglements, and only differ by the number of monomers per chain. This corresponds to changing the crosslink-to-monomer ratio, which is often done in experiments<sup>[42–43]</sup>. We conduct our simulations in a periodic computational domain. In the simulations with microgel networks, we choose a domain size in the range from  $100 \times 100 \times 100$  to  $170 \times 170 \times 170$  such that any interactions of the microgel with its periodical images are prevented. The domain size for single chain simulations is  $20 \times 20 \times 20$ . At the beginning of the simulations, we equilibrate the microgel network in solvent until a steady state situation is reached.

### 3 Results and discussion

#### 3.1 Single chain model

Neutral poly ( $N$ -isopropylacrylamide) (PNIPAM) gels are composed of polymer chains that exhibit flexible behavior<sup>[44]</sup>. We use this property as a guiding criterion for constructing our mesoscale model for a polymer chain. Flory’s theory allows us to characterize the flexibility of individual polymer chains in a dilute solution in terms of the relation between the end-to-end distance  $R_{\text{end}}$  and the number of monomers  $N$ . This relation is given by

$$R_{\text{end}} \sim l_k(N - 1)^v,$$

where  $l_k$  is the Kuhn length, and  $\nu$  is Flory's exponent equal to  $3/5$  for flexible, self-avoiding chains in good solvent<sup>[45]</sup>.

When the bead-spring model is used without bending stiffness, we reproduce the flexible behavior of a polymer chain with just a few beads per chain. In Fig. 2(a), we show a log-log plot of  $R_{\text{end}}$  as a function of the number of beads for chains with different  $k_{\text{bend}}$  and the chain solvent repulsion  $a = 20$ . The lines in the figure correspond to  $\nu = 3/5$ . When  $k_{\text{bend}} = 0$ , the bead-spring model conforms to the expected scaling behavior, even for very short chains. Including bending stiffness, however, leads to deviations for chains with a small number of beads (see  $k_{\text{bend}} = 5$  and  $k_{\text{bend}} = 10$  in Fig. 2(a)). These chains behave as flexible chains only if the number of beads in the chain is sufficiently large. In Fig. 2(b), we show the dependence of the minimum number of beads in the chain  $N_{\text{min}}$  for the chain to be flexible as a function of the bending stiffness. This number increases as  $k_{\text{bend}}$  increases. Hence, chains with  $N > N_{\text{min}}$  behave as flexible chains, whereas chains with  $N < N_{\text{min}}$  are semi-flexible. Note that in our mesoscale microgel model, we are interested in using shorter chains to reduce the size of the system and accelerate the simulations.

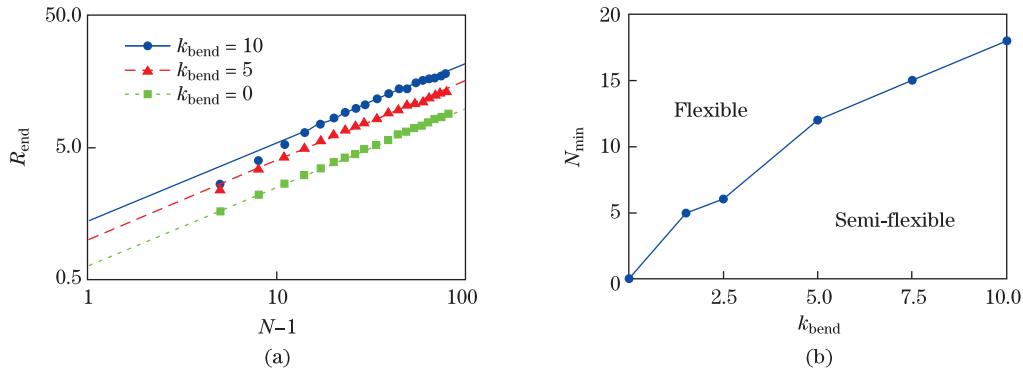


**Fig. 2** (a) End-to-end distance of linear chains with different  $k_{\text{bend}}$  and  $a = 20$ . The points show simulation data, whereas the lines represent the Flory theory scaling behavior for flexible chains. As the bending stiffness increases, longer chains deviate from the flexible behavior. (b) Minimum chain length for which chains follow flexible behavior as a function of the chain bending stiffness. The line separates parameter space for the flexible and semi-flexible polymer chains. For stiffer chains, a longer length is required to recover flexible behavior

In addition to changing the values of  $N_{\text{min}}$ , bending stiffness also affects the magnitude of the Kuhn length, which represents the effective length of orientationally independent segments within a polymer chain. For  $k_{\text{bend}} = 0$ , the Kuhn length is relatively short and is equal to about 0.6, which is the equilibrium length  $r_{\text{eq}}$  for stretching springs connecting the beads in the chain. The addition of bending stiffness leads to an increased Kuhn length which increases nearly linearly with  $k_{\text{bend}}$  within the tested range (see Fig. 3). As we show below, larger values of Kuhn length are critical for modeling highly porous swollen gels.

### 3.2 Microgel swelling

Hydrogels are characterized by a high porosity in good solvents<sup>[44,46]</sup>, which plays a fundamental role in gel transport properties, mechanics, and swelling kinetics. It is, therefore, important that our mesoscale microgel model can exhibit the relevant values of porosity in good solvent conditions.

In Fig. 4(a), we plot the gel porosity  $P$  as a function of  $k_{\text{bend}}$  for chains with different  $N$ . To determine the microgel porosity, we first measure the microgel volume  $V$  by constructing a surface mesh enclosing the microgel network (see Fig. 4(b))<sup>[47]</sup>. The surface mesh is defined using a spherical probe with a radius of about half of the microgel mesh size. We then calculate

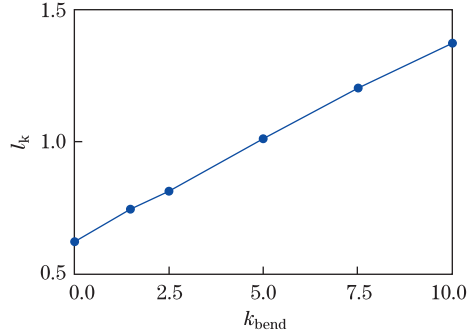


**Fig. 3** Kuhn length monotonically increases with bending stiffness. With increasing  $k_{\text{bend}}$ , the number of beads in each Kuhn segment increases. When  $k_{\text{bend}} = 0$ , the Kuhn length corresponds to one bond length, which is 0.6 in DPD units

microgel porosity based on the number of solvent beads located within the surface mesh. We find that  $P$  increases with chain length. However, when  $k_{\text{bend}} = 0$ , the porosity does not exceed

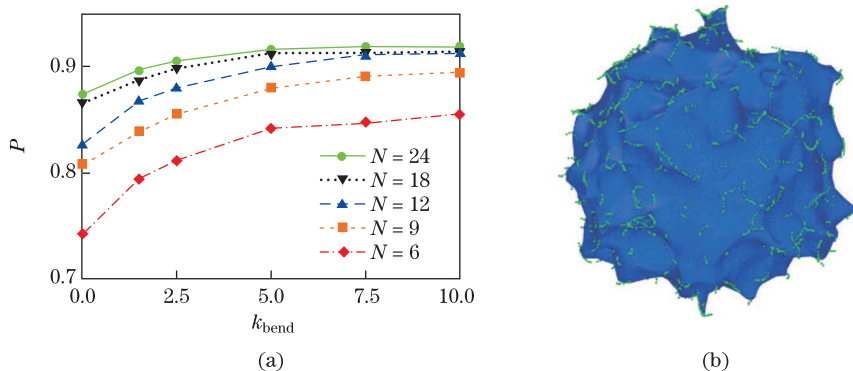


**Fig. 4** (a) Porosity of spherical microgels composed of chains with different length and  $a = 20$  as a function of the chain bending stiffness. (b) Triangulated surface mesh enclosing a microgel network. The mesh surface is shown in blue and the gel beads are shown in green (color online)

0.87 even for relatively long chains with  $N = 24$ . A further increase in the chain length can lead to higher porosity. However, this also significantly extends the computation time, as the domain size scales as  $N^3$ .

Long computational times can be avoided by noting that  $P$  can be increased by using shorter chains with a greater  $k_{\text{bend}}$  and, thus, a greater Kuhn length. Indeed, we find that when  $k_{\text{bend}} = 10$ , the porosity is about 0.95 for the chains with  $N = 24$ , which is close to typical experimental values for hydrogels. Furthermore, these chains behave as flexible chains, which is also typical in experiments. We, therefore, use the chains with  $k_{\text{bend}} = 10$  in our mesoscale model. Using chains with higher bending stiffness will further increase microgel porosity. However, this will require longer chains in order to ensure that fully flexible behavior is maintained, which in turn will lead to excessive computational time.

We conduct simulations, in which we place a spherical microgel network in the solutions with different solvency that is varied by changing the network solvent repulsion coefficient  $a$ . Larger values of  $a$  correspond to bad solvents, whereas lower values of  $a$  correspond to good

solvents. At each  $a$ , we calculate the network porosity (see Fig. 5(a)) for gels with different  $N$ . In bad solvents, all microgel networks have a nearly zero porosity, indicating that the microgel expels practically all of the solvent and adopts a nearly collapsed state. Note, that  $P > 0$ , which agrees with what is found in experiments<sup>[48]</sup>. In good solvents, the microgel swells, resulting in values of  $P$  approaching 0.95 for large  $N$ .

The microgel volume change, as the solvent changes from good to bad, strongly depends on  $N$ . For  $N = 6$ , the volume increases approximately 7 times, when the microgel changes from the collapsed state to the swollen state. For  $N = 24$ , the volume increases about 30 times between collapsed and swollen states. We find that, as the chain length increases, the volume-phase transition becomes sharper, as indicated by the greater values of the porosity gradient,  $|\Delta P/\Delta a|$ , for the microgels with longer chains in Fig. 5(b). This behavior is related to the microgel softening due to the decreasing crosslink density  $\rho_c = \eta/V_a$  in microgels with larger  $N$ . Here,  $\eta$  is the total number of crosslinks, and  $V_a$  is the gel volume for a given value of  $a$ . This result is in qualitative agreement with expectations from Flory-Rehner's theory of polymer gels<sup>[49]</sup>.

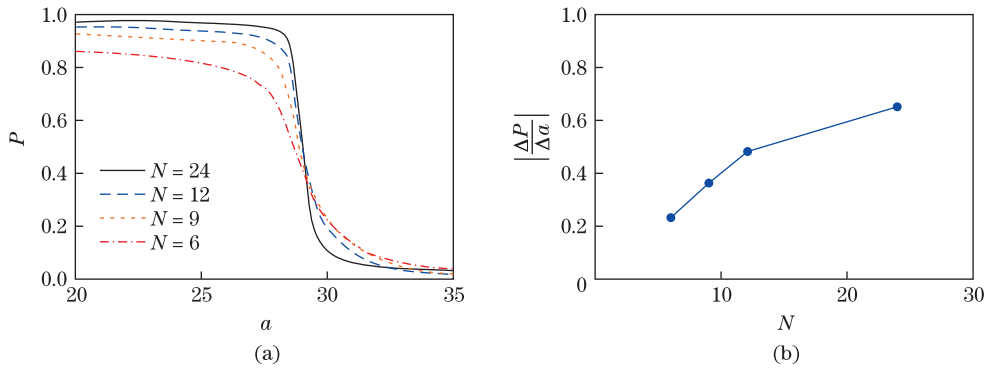


**Fig. 5** (a) Swelling curves in terms of porosity and network-solvent repulsion for spherical microgels with different chain lengths. (b) Derivative of network porosity with respect to network-solvent repulsion near the swelling transition. The magnitude of the derivative increases with chain length, indicating a sharper volume phase transition

Larger volume changes can be also obtained by using polymer chains with greater bending stiffness. In good solvent, stiffer chains lead to a higher microgel porosity, whereas in bad solvent conditions, the size of the collapsed gels is nearly insensitive to  $k_{\text{bend}}$  and is mostly defined by the excluded volume of the chains.

### 3.3 Bulk modulus

We measure the bulk modulus of our mesoscale gels by quasi-statically varying the total osmotic pressure imposed on the microgel network. To change the osmotic pressure, we create a semi-permeable spherical shell around the microgel (see Fig. 6). The spherical shell interacts with the gel particles via a harmonic potential, while the solvent particles are allowed to pass freely through the shell. Varying the radius of the spherical shell, thus, effectively mimics a change in the osmotic pressure. For each solvency  $a$ , we vary the radius of the semi-permeable shell, and evaluate the corresponding network volume and pressure. To find the microgel volume  $V$ , we construct a surface mesh around the gel. The network pressure is calculated as

$$\Pi_{\text{network}} = W(\sigma_{xx}^{\text{ave}} + \sigma_{yy}^{\text{ave}} + \sigma_{zz}^{\text{ave}})/(3V),$$

where  $W$  is the number of microgel beads in the network, and  $\sigma_{ii}^{\text{ave}}$  ( $i = x, y, z$ ) are the average normal stresses per bead in the  $x$ -,  $y$ -, and  $z$ -directions. The stress is averaged over all beads in the microgel network.

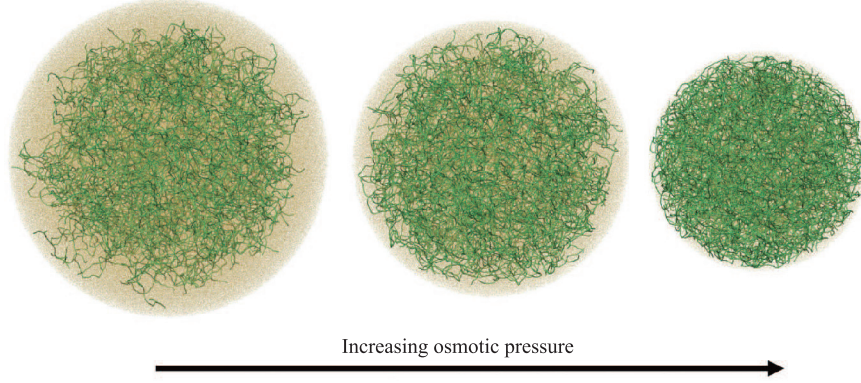


**Fig. 6** Illustration of bulk modulus measurements. The images show the microgel inside a spherical shell. The yellow points represent solvent beads, while the green points represent microgel beads. Decreasing the radius of the semi-permeable shell increases the osmotic pressure on the microgel (color online)

Figure 7(b) shows the resultant bulk moduli  $K$  for microgels with different  $N$  through the volume phase transition. The pressure is calculated for different values of solvency  $a$  in the linear region of microgel compression, where  $\Pi_{\text{network}}$  is a linear function of  $V$  (see the inset in Fig. 7(a)). The variation of  $\Pi_{\text{network}}$  with  $V$  in this linear region is used to evaluate the microgel bulk modulus as follows:

$$K = V \frac{\Delta \Pi_{\text{network}}}{\Delta V}.$$

This procedure is repeated for different  $a$ , covering the entire range of the microgel swelling transition.

Figure 7(b) shows the resultant bulk modulus  $K$  for the microgels with different  $N$  through the volume phase transition. We find that the bulk modulus monotonically increases as the solvency decreases. This increase in  $K$  is related to a decrease in the microgel porosity and an increase in the crosslink density  $\rho_c$  as  $a$  increases. In a good solvent with  $a < 25$  (swollen state), the bulk modulus decreases with  $N$ . In this case, increasing  $N$  decreases the crosslink density, resulting in gel softening. This softening of the microgels with increasing  $N$  also leads to a sharper volume-phase transition (see Fig. 5).

Analytically, the microgel bulk modulus can be evaluated with the Flory-Rehner theory, which postulates that, for nonionic gels, the total osmotic pressure  $\Pi_{\text{network}}$  is composed of a mixing osmotic pressure  $\Pi_{\text{mix}}$  due to polymer-solvent mixing and an elastic osmotic pressure  $\Pi_e$  due to network elasticity<sup>[49]</sup>. In equilibrium with pure solvent,  $\Pi_{\text{mix}}$  balances  $\Pi_e$ . Using that

$$K = \phi \frac{\partial \Pi_{\text{network}}}{\partial \phi}$$

and Flory's descriptions of  $\Pi_{\text{mix}}$  and  $\Pi_e$ , we can obtain an expression for the microgel bulk modulus as follows:

$$K = \frac{k_B T}{v_s} \left( \frac{N_c}{V_o} v_s \left( \frac{1}{2} \left( \frac{\phi}{\phi_o} \right) - \left( \frac{\phi}{2\phi_o} \right)^{1/3} \right) + \frac{\phi^2}{1-\phi} - 2\chi\phi^2 \right),$$

where  $\phi = 1 - P$  is the polymer volume fraction,  $N_c/V_o$  is the number of polymer chains in the preparation state per volume, which corresponds to the nearly collapsed state in our simulations,  $v_s$  is the molar volume of the solvent,  $\phi_o$  is the volume fraction in the preparation



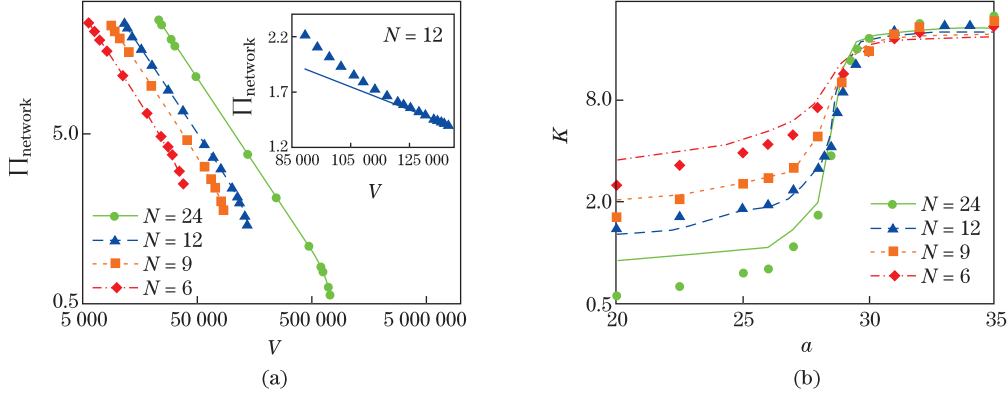


**Fig. 7** (a) Network pressure as a function of the microgel volume for different chain lengths throughout the volume phase transition. The inset shows  $\Pi_{\text{network}}$  as a function of  $V$  for  $N = 12$  and  $a = 20$ . The solid line in the inset shows slope of the linear deformation region. (b) Bulk modulus from simulations (symbols) and corresponding fits to Flory-Rehner’s theory (lines). In bad solvent, all microgels have the same bulk modulus. In good solvent, the microgels with longer chain lengths have a higher porosity and are thus softer

state, and  $\chi$  is the solvency parameter. For our microgels, we evaluate the solvent molar volume as

$$v_s = r_c^3 N_A / \rho,$$

where  $r_c$  is the cutoff radius of the DPD potential,  $N_A$  is Avogadro’s number, and  $\rho$  is the density in our simulations<sup>[50]</sup>.

We fit our simulation results for  $K$  versus  $a$  with Flory-Rehner’s theory, using the relation between  $\Pi_{\text{network}}$ , and thus  $\phi$ , with  $a$ . We consider the solvency parameter as a function of the polymer volume fraction

$$\chi = \chi_0 + \chi_1 \phi + \chi_2 \phi^2$$

and set  $k_B T / v_s$ ,  $N_c v_s / V_o$ ,  $\chi_0$ ,  $\chi_1$ , and  $\chi_2$  as the fitting parameters. In our simulations, the number of polymer chains per volume in the preparation state is  $N_c / V_o \sim 0.25$  chains per unit volume. The obtained values of the fitting parameters are summarized in Table 1. We find that the values are nearly independent of the chain length  $N$ .

**Table 1** Fitting parameters from bulk modulus fits

$N$	$k_B T / v_s$	$N_c v_s / V_o$	$\chi_0$	$\chi_1$	$\chi_2$
6	$1.02 \times 10^{-21}$	$4.88 \times 10^{22}$	0.491 02	0.050 18	0.502 64
9	$1.05 \times 10^{-21}$	$4.90 \times 10^{22}$	0.509 56	0.050 97	0.507 83
12	$9.97 \times 10^{-22}$	$5.28 \times 10^{22}$	0.513 57	0.050 91	0.499 95
24	$1.08 \times 10^{-21}$	$5.09 \times 10^{22}$	0.507 25	0.050 00	0.497 55

The resulting fits to our bulk modulus data correctly describe our simulation results (see Fig. 7(b)). We note that if the fits are performed under the assumption that  $\chi$  is linearly dependent on  $\phi$ , good agreement between our simulations and the theory cannot be obtained. Thus, the quadratic dependence of  $\chi$  on  $\phi$  is essential. This is consistent with previous experiments, and suggests that many-body interactions become important near the swelling transition<sup>[49]</sup>.

Using the results for  $\chi$  from the fits, we can establish how this parameter depends on the network-solvent repulsion coefficient  $a$ . This is shown for different  $N$  in Fig. 8. We find that the

$\chi$ - $a$  dependence is not sensitive to the value of  $N$ . Furthermore, in good solvents, the solvency parameter is about 0.5, whereas in bad solvents, it increases to about 1. This behavior agrees reasonably well with the experimental data<sup>[51–53]</sup>.

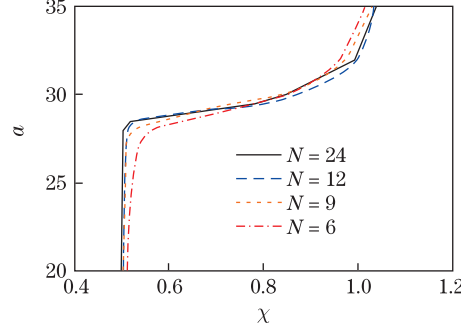


**Fig. 8** Relationship between the Flory-Huggins solvency parameter and the network-solvent repulsion in DPD simulations

### 3.4 Swelling kinetics

When the gel undergoes a volume transition, the kinetics of this process is defined by a balance among osmotic pressure, gel elasticity, and viscous drag due to the solvent penetrating in or out of the gel network. The swelling kinetics of a spherical gel can be analyzed analytically<sup>[54]</sup>. The change in the gel radius is given by

$$\Delta r(t) = \Delta r_o \frac{6}{\pi^2} \sum_n n^{-2} e^{-n^2 t / \tau_s},$$

where  $\Delta r_o$  is the total increase in the radius defined by

$$\Delta r_o = r_{\text{final}} - r_{\text{ini}}.$$

In the above equation,  $r_{\text{final}}$  and  $r_{\text{ini}}$  are the final and initial equilibrated gel radii, respectively,  $\tau_s$  is the swelling time constant, and  $t$  is time. The swelling time constant is given by

$$\tau_s = r_{\text{final}}^2 / D.$$

In the above equation,  $D$  is the collective diffusion of the gel characterizing its elastic relaxation in a viscous solvent, and is expressed by

$$D = (K + 4\mu/3)/f,$$

where  $K$  is the bulk modulus,  $\mu$  is the shear modulus, and  $f$  is the friction coefficient between the polymer network and the fluid.

To examine whether our mesoscale gel model can properly describe swelling kinetics, we simulate the swelling of a spherical microgel that is initially in the collapsed state ( $a = 35$ ). At  $t = 0$ , the collapsed gel is placed in a good solvent ( $a = 20$ ). In our simulations, we track how the microgel radius changes as the microgel undergoes swelling in good solvent. The results of the simulations for different chain lengths  $N$  are shown in Fig. 9(a). We fit the simulation data to Tanaka’s theory to determine the relaxation constant  $\tau_s$  and the corresponding value of the collective diffusion coefficient  $D$ , which are given in Table 2. The data indicates that  $\tau_s$  increases roughly proportional to  $N^2$ , whereas the collective diffusion  $D$  decreases with the increase in  $N$ <sup>[55]</sup>. As a result, networks with longer chains swell slower than the networks with smaller chains. Figure 9(a) shows close agreement between the theoretical results and the simulation results for all  $N$ , indicating that our microgel model can properly capture not only microgel mechanics but also microgel interactions with the viscous solvent.

**Table 2** Microgel swelling/collapsing kinetics parameters

$N$	Gel swelling		Gel collapsing	
	$D$	$\tau_s$	$D$	$\tau_s$
6	1.957	220	0.567	210
9	1.721	430	0.559	280
12	1.640	620	0.537	360
24	1.162	2 300	0.344	900

We also examine the microgel kinetics during deswelling. In this scenario, the swollen spherical gel ( $a = 20$ ) is introduced to a bad solvent ( $a = 35$ ). The time evolution of the microgel size is shown in Fig. 9(b). We find that the deswelling simulation data can also be fitted to Tanaka's theory, although the agreement is somewhat less accurate when compared with the swelling process. Comparing the fitting parameters in Table 2, we find that the relaxation time is considerably shorter for deswelling microgels, especially for longer chain lengths. This can be expected since the relaxation time is proportional to  $r_{\text{final}}^2$ , which is much smaller for collapsed microgels than for swollen microgels. We also find that the collective diffusion  $D$  is about 3 times smaller for deswelling microgels, indicating differences in the internal structure of the microgels during the swelling and deswelling transitions.

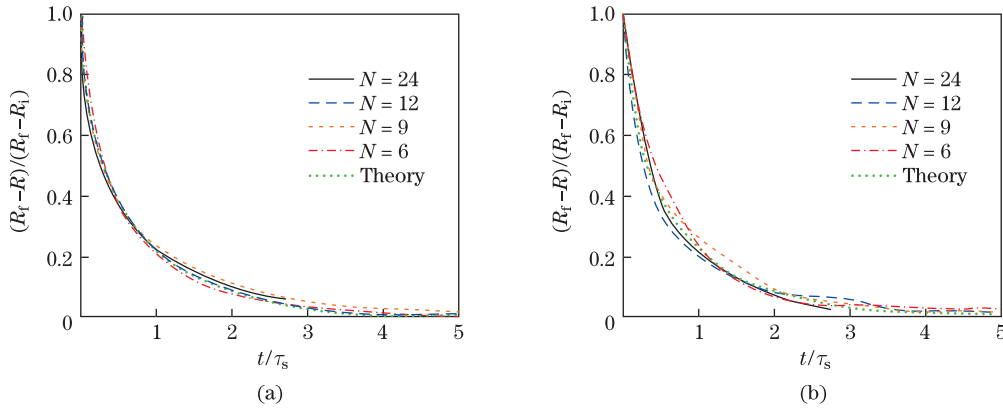


**Fig. 9** (a) Swelling kinetics for spherical microgels transitioning from the collapsed state to the swollen state. (b) Swelling kinetics results for microgels transitioning from the swollen state to the collapsed state. The theoretical line shows the prediction of Tanaka's theory for the swelling of a spherical gel

Figure 10 illustrates the microgels that undergo swelling (top row) and deswelling (bottom row) transitions. During swelling, the particle gradually increases in size while maintaining a nearly homogeneous structure (see Fig. 10(a)). In contrast, during deswelling, the microgel exhibits a remarkably different internal structure at intermediate times. Our simulations indicate that the deswelling from a fully swollen state proceeds through network coarsening that manifests as formation of chain bundles at the outskirts of the microgels (see Fig. 10(b)). Similar coarsening behavior has been reported for isochore phase separation in hydrogels<sup>[56]</sup>. Eventually, however, the microgel volume decreases and the solvent is expelled, allowing the microgel to shrink to its collapsed size. Note that this process is different from the rapid deswelling of macroscopic gel, whereby a skin of collapsed gels is formed on the outer gel surface. This dense skin prevents solvent transfer from the hydrogel interior, thereby delaying the gel deswelling<sup>[57]</sup>.

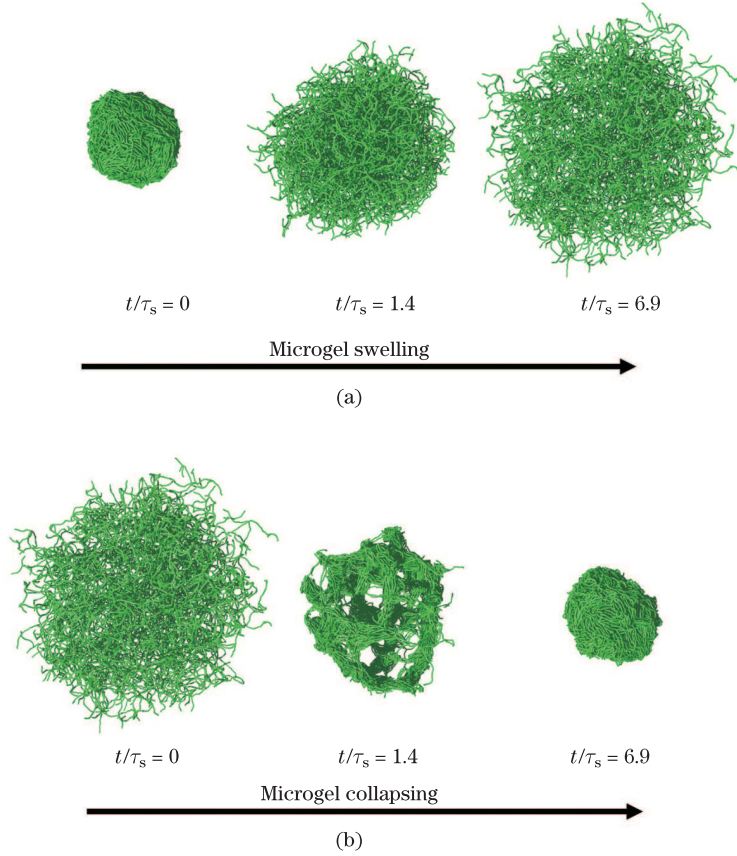


**Fig. 10** Simulation snapshots illustrating a microgel network with  $N = 12$  during (a) swelling and (b) deswelling. The bad and good solvent conditions are modeled with  $a = 35$  and  $a = 20$ , respectively. Time is normalized by the corresponding swelling time constant (color online)

## 4 Conclusions

We have examined the mechanics and swelling kinetics of neutral microgel particles using a mesoscale polymer network model. The model network is immersed in an explicit viscous solvent modeled using dissipative particle dynamics. We alter the solvency by changing the repulsion between the network and the solvent. To prevent chains from crossing each other, we employ a bond-bond repulsive potential. To model sufficiently large microgel networks, we identify single chain parameters leading to experimentally realistic microgel properties. We find that, to model swollen microgels with high porosity, bending stiffness needs to be incorporated into the polymer chains to increase their Kuhn length. This imposes a limitation on the minimum polymer chain length when flexible chain mechanics is required.

We show that microgels undergo a continuous volume transition when the solvency is changed. In bad solvents, the networks contract to a nearly collapsed state, whereas in good solvents, the microgels swell with a porosity that increases proportionally to the chain length. Microgels with higher porosity are characterized by a sharper volume transition. To probe the effect of the volume-phase transition on the microgel mechanics, we employ our simulation model to obtain the microgel bulk modulus. We find that the bulk modulus changes monotonically through the volume transition. In the collapsed state, the bulk modulus is independent of the chain length, and is defined by the chain-chain repulsion. In swollen networks, the modulus

decreases with increasing porosity and decreasing crosslink density. We fit our bulk modulus data to the Flory-Rehner theory, and show that our mesoscale model is in good agreement with the theory. From the fitting, we obtain the Flory-Huggins solvency parameter. This procedure allows establishing a relation between the solvency parameter and the solvent-network repulsion parameter. We find that the solvency parameter exhibits a quadratic dependence on the polymer volume fraction, which is consistent with the experimental results, reflecting the importance of many-body interactions through the swelling transition.

Finally, we study the swelling kinetics of our microgel particles. Our simulations show close agreement to Tanaka's theory for spherical gels. This result indicates that the mesoscale model can properly capture the hydrodynamics of network-solvent interactions. Importantly, we find that, during swelling, microgels preserve a nearly homogeneous internal structure, whereas rapid deswelling leads to the formation of chain bundles in the outskirts of the particle and network coarsening. The difference in internal microgel structure is manifested by different kinetic constants, characterizing the speed of the swelling and deswelling transitions. In its current implementation, our mesoscale model is limited to modeling microgels exhibiting a continuous volume phase transition. Thus, our microgel model cannot simulate gels with a negative Poisson ratio and discontinuity in the bulk modulus, which are observed near the critical volume phase transition for certain microgels<sup>[58]</sup>. More elaborate chain-chain and chain-solvent interactions need to be integrated into the model to capture these effects, which is an important direction for future model development.

## References

- [1] Hoffman, A. S. Hydrogels for biomedical applications. *Advanced Drug Delivery Reviews*, **64**, 18–23 (2012)
- [2] Chaudhuri, O., Gu, L., Klumpers, D., Darnell, M., Bencherif, S. A., Weaver, J. C., Huebsch, N., Lee, H. P., Lippens, E., and Duda, G. N. Hydrogels with tunable stress relaxation regulate stem cell fate and activity. *Nature Materials*, **15**, 326 (2016)
- [3] Shin, S. R., Bae, H., Cha, J. M., Mun, J. Y., Chen, Y. C., Tekin, H., Shin, H., Farshchi, S., Dokmeci, M. R., and Tang, S. Carbon nanotube reinforced hybrid microgels as scaffold materials for cell encapsulation. *ACS Nano*, **6**, 362–372 (2011)
- [4] Kim, M. Y. and Kim, J. Y. Chitosan microgels embedded with catalase nanozyme-loaded mesocellular silica foam for glucose-responsive drug delivery. *ACS Biomaterials Science and Engineering*, **3**, 572–578 (2017)
- [5] Utech, S., Prodanovic, R., Mao, A. S., Ostafe, R., Mooney, D. J., and Weitz, D. A. Microfluidic generation of monodisperse, structurally homogeneous alginate microgels for cell encapsulation and 3D cell culture. *Advanced Healthcare Materials*, **4**, 1628–1633 (2015)
- [6] Hardin, J. O., Fernandez-Nieves, A., Martinez, C. J., and Milam, V. T. Altering colloidal surface functionalization using DNA encapsulated inside monodisperse gelatin microsphere templates. *Langmuir*, **29**, 5534–5539 (2013)
- [7] Brown, A. C., Stabenfeldt, S. E., Ahn, B., Hannan, R. T., Dhada, K. S., Herman, E. S., Stefanelli, V., Guzzetta, N., Alexeev, A., Lam, W. A., Lyon, L. A., and Barker, T. H. Ultrasoft microgels displaying emergent platelet-like behaviours. *Nature Materials*, **13**, 1108–1114 (2014)
- [8] Douglas, A. M., Fragkopoulos, A. A., Gaines, M. K., Lyon, L. A., Fernandez-Nieves, A., and Barker, T. H. Dynamic assembly of ultrasoft colloidal networks enables cell invasion within restrictive fibrillar polymers. *Proceedings of the National Academy of Sciences*, **114**, 885–890 (2017)
- [9] Wu, S. H., Duan, B., Qin, X. H., and Butcher, J. T. Nanofiber-structured hydrogel yarns with pH-response capacity and cardiomyocyte-drivability for bio-microactuator application. *Acta Biomaterialia*, **60**, 144–153 (2017)
- [10] Ye, C. H., Nikolov, S. V., Calabrese, R., Dindar, A., Alexeev, A., Kippelen, B., Kaplan, D. L., and Tsukruk, V. V. Self-(un)rolling biopolymer microstructures: rings, tubules, and helical tubules from the same material. *Angewandte Chemie International Edition*, **54**, 8490–8493 (2015)

- 
- [11] Ye, C. H., Nikolov, S. V., Geryak, R. D., Calabrese, R., Ankner, J. F., Alexeev, A., Kaplan, D. L., and Tsukruk, V. V. Bimorph silk microsheets with programmable actuating behavior: experimental analysis and computer simulations. *ACS Applied Materials and Interfaces*, **8**, 17694–17706 (2016)
- [12] Vikram, S. A. and Sitti, M. Targeted drug delivery and imaging using mobile milli/microrobots: a promising future towards theranostic pharmaceutical design. *Current Pharmaceutical Design*, **22**, 1418–1428 (2016)
- [13] Nikolov, S. V., Yeh, P. D., and Alexeev, A. Self-propelled microswimmer actuated by stimulus-sensitive bilayered hydrogel. *ACS Macro Letters*, **4**, 84–88 (2015)
- [14] Masoud, H., Bingham, B. I., and Alexeev, A. Designing maneuverable micro-swimmers actuated by responsive gel. *Soft Matter*, **8**, 8944–8951 (2012)
- [15] Du, H. B. and Qian, X. H. Molecular dynamics simulations of PNIPAM-co-PEGMA copolymer hydrophilic to hydrophobic transition in NaCl solution. *Journal of Polymer Science Part B: Polymer Physics*, **49**, 1112–1122 (2011)
- [16] Kang, M. K. and Huang, R. A variational approach and finite element implementation for swelling of polymeric hydrogels under geometric constraints. *Journal of Applied Mechanics*, **77**, 061004 (2010)
- [17] Mills, Z. G., Mao, W. B., and Alexeev, A. Mesoscale modeling: solving complex flows in biology and biotechnology. *Trends in Biotechnology*, **31**, 426–434 (2013)
- [18] Yeh, P. D. and Alexeev, A. Mesoscale modelling of environmentally responsive hydrogels: emerging applications. *Chemical Communications*, **51**, 10083–10095 (2015)
- [19] Espanol, P. and Warren, P. Perspective: dissipative particle dynamics. *The Journal of Chemical Physics*, **146**, 150901 (2017)
- [20] Groot, R. D. and Warren, P. B. Dissipative particle dynamics: bridging the gap between atomistic and mesoscopic simulation. *Journal of Chemical Physics*, **107**, 4423–4435 (1997)
- [21] Hoogerbrugge, P. J. and Koelman, J. M. V. A. Simulating microscopic hydrodynamic phenomena with dissipative particle dynamics. *Europhysics Letters*, **19**, 155–160 (1992)
- [22] Espanol, P. and Warren, P. Statistical-mechanics of dissipative particle dynamics. *Europhysics Letters*, **30**, 191–196 (1995)
- [23] Glotzer, S. C. and Paul, W. Molecular and mesoscale simulation methods for polymer materials. *Annual Review of Materials Research*, **32**, 401–436 (2002)
- [24] Groot, R. D. and Rabone, K. L. Mesoscopic simulation of cell membrane damage, morphology change and rupture by nonionic surfactants. *Biophysical Journal*, **81**, 725–736 (2001)
- [25] Chen, S., Phan-Thien, N., Fan, X. J., and Khoo, B. C. Dissipative particle dynamics simulation of polymer drops in a periodic shear flow. *Journal of Non-Newtonian Fluid Mechanics*, **118**, 65–81 (2004)
- [26] Fedosov, D. A., Karniadakis, G. E., and Caswell, B. Dissipative particle dynamics simulation of depletion layer and polymer migration in micro and nanochannels for dilute polymer solutions. *Journal of Chemical Physics*, **128**, 144903 (2008)
- [27] Spenley, N. A. Scaling laws for polymers in dissipative particle dynamics. *Europhysics Letters*, **49**, 534–540 (2000)
- [28] Ripoll, M., Ernst, M. H., and Espanol, P. Large scale and mesoscopic hydrodynamics for dissipative particle dynamics. *Journal of Chemical Physics*, **115**, 7271–7284 (2001)
- [29] Lee, M. T., Vishnyakov, A. N., and Alexander, V. Modeling proton dissociation and transfer using dissipative particle dynamics simulation. *Journal of Chemical Theory and Computation*, **11**, 4395–4403 (2015)
- [30] Li, N. K., Kuang, H. H., Fuss, W. H., and Yingling, Y. G. Salt responsive morphologies of ssDNA-based triblock polyelectrolytes in semi-dilute regime: effect of volume fractions and polyelectrolyte length. *Macromolecular Rapid Communications*, **38**, 1700422 (2017)
- [31] Groot, R. D. Electrostatic interactions in dissipative particle dynamics-simulation of polyelectrolytes and anionic surfactants. *Journal of Chemical Physics*, **118**, 11265–11277 (2003)

- 
- [32] Ibergay, C., Malfreyt, P., and Tildesley, D. J. Electrostatic interactions in dissipative particle dynamics: toward a mesoscale modeling of the polyelectrolyte brushes. *Journal of Chemical Theory and Computation*, **5**, 3245–3259 (2009)
- [33] Boek, E. S., Coveney, P. V., Lekkerkerker, H. N. W., and van der Schoot, P. Simulating the rheology of dense colloidal suspensions using dissipative particle dynamics. *Physical Review E*, **55**, 3124–3133 (1997)
- [34] Symeonidis, V., Karniadakis, G. E., and Caswell, B. Dissipative particle dynamics simulations of polymer chains: scaling laws and shearing response compared to DNA experiments. *Physical Review Letters*, **95**, 076001 (2005)
- [35] Ganzenmuller, G. C., Hiermaier, S., and Steinhauser, M. O. Shock-wave induced damage in lipid bilayers: a dissipative particle dynamics simulation study. *Soft Matter*, **7**, 4307–4317 (2011)
- [36] Chu, X. L., Aydin, F., and Meenakshi, D. Modeling interactions between multicomponent vesicles and antimicrobial peptide-inspired nanoparticles. *ACS Nano*, **10**, 7351–7361 (2016)
- [37] Pivkin, I. V., Peng, Z. L., Karniadakis, G. E., Buffet, P. A., Dao, M., and Suresh, S. Biomechanics of red blood cells in human spleen and consequences for physiology and disease. *Proceedings of the National Academy of Sciences of the United States of America*, **114**, E4521 (2017)
- [38] Masoud, H. and Alexeev, A. Permeability and diffusion through mechanically deformed random polymer networks. *Macromolecules*, **43**, 10117–10122 (2010)
- [39] Masoud, H. and Alexeev, A. Controlled release of nanoparticles and macromolecules from responsive microgel capsules. *ACS Nano*, **6**, 212–219 (2012)
- [40] Sirk, T. W., Slizoberg, Y. R., Brennan, J. K., Lisal, M., and Andzelm, J. W. An enhanced entangled polymer model for dissipative particle dynamics. *Journal of Chemical Physics*, **136**, 134903 (2012)
- [41] Tarjan, R. Depth-first search and linear graph algorithms. *SIAM Journal on Computing*, **1**, 146–160 (1972)
- [42] Pelaez-Fernandez, M., Souslov, A., Lyon, L. A., Goldbart, P. M., and Fernandez-Nieves, A. Impact of single-particle compressibility on the fluid-solid phase transition for ionic microgel suspensions. *Physical Review Letters*, **114**, 098303 (2015)
- [43] Senff, H. and Richtering, W. Influence of cross-link density on rheological properties of temperature-sensitive microgel suspensions. *Colloid and Polymer Science*, **278**, 830–840 (2000)
- [44] Fernandez-Nieves, A., Wyss, H., Mattsson, J., and Weitz, D. A. *Microgel Suspensions: Fundamentals and Applications*, John Wiley and Sons, Singapore (2011)
- [45] De Gennes, P. G. *Scaling Concepts in Polymer Physics*, Cornell University Press, New York (1979)
- [46] Annabi, N., Nichol, J. W., Zhong, X., Ji, C. D., Koshy, S., Khademhosseini, A., and Dehghani, F. Controlling the porosity and microarchitecture of hydrogels for tissue engineering. *Tissue Engineering Part B: Reviews*, **16**, 371–383 (2010)
- [47] Stukowski, A. Visualization and analysis of atomistic simulation data with OVITO—the open visualization tool. *Modelling and Simulation in Materials Science and Engineering*, **18**, 015012 (2009)
- [48] Sierra-Martin, B., Laporte, Y., South, A. B., Lyon, L. A., and Fernandez-Nieves, A. Bulk modulus of poly (*N*-isopropylacrylamide) microgels through the swelling transition. *Physical Review E*, **84**, 011406 (2011)
- [49] Hirotsu, S. Static and time-dependent properties of polymer gels around the volume phase transition. *Phase Transitions: A Multinational Journal*, **47**, 183–240 (1994)
- [50] Slizoberg, Y. R., Andzelm, J. W., Brennan, J. K., Vanlandingham, M. R., Pryamitsyn, V., and Ganesan, V. Modeling viscoelastic properties of triblock copolymers: a DPD simulation study. *Journal of Polymer Science Part B: Polymer Physics*, **48**, 15–25 (2010)
- [51] Hirotsu, S. Coexistence of phases and the nature of first-order phase transition in poly-*N*-isopropylacrylamide gels. *Responsive Gels: Volume Transitions II*, Springer, Berlin, Heidelberg, 1–26 (1993)
- [52] Lopez-Leon, T. and Fernandez-Nieves, A. Macroscopically probing the entropic influence of ions: deswelling neutral microgels with salt. *Physical Review E*, **75**, 011801 (2007)

- [53] Fernandez-Barbero, A., Fernandez-Nieves, A., Grillo, I., and Lopez-Cabarcos, E. Structural modifications in the swelling of inhomogeneous microgels by light and neutron scattering. *Physical Review E*, **66**, 051803 (2002)
- [54] Tanaka, T. and Fillmore, D. J. Kinetics of swelling of gels. *The Journal of Chemical Physics*, **70**, 1214–1218 (1979)
- [55] Geissler, E., Bohidar, H. B., and Hecht, A. M. Collective diffusion in semi-dilute gels at the theta temperature. *Macromolecules*, **18**, 949–953 (1985)
- [56] Shibayama, M., Morimoto, M., and Nomura, S. J. Phase separation induced mechanical transition of poly (*N*-isopropylacrylamide) water isochore gels. *Macromolecules*, **27**, 5060–5066 (1994)
- [57] Patil, N., Soni, J., Ghosh, N., and De, P. Swelling-induced optical anisotropy of thermoresponsive hydrogels based on poly (2-(2-methoxyethoxy) ethyl methacrylate): deswelling kinetics probed by quantitative Mueller matrix polarimetry. *The Journal of Physical Chemistry B*, **116**, 13913–13921 (2012)
- [58] Hirotsu, S. Softening of bulk modulus and negative Poisson’s ratio near the volume phase transition of polymer gels. *The Journal of Chemical Physics*, **94**, 3949–3957 (1991)